



RESEARCH LETTER

10.1002/2015GL065489

Special Section:

First Results from the MAVEN Mission to Mars

Key Points:

- Retrieved CO₂ densities at 170 km vary by a factor of about 2.5
- On average, N₂/CO₂ increases from 4% at 130 km to 12% at 200 km
- Mean Martian upper atmospheric temperature over the sampled time frame is 324 (±) 22 K

Supporting Information:

- Figures S1–S3

Correspondence to:

J. S. Evans,
evans@cpi.com

Citation:

Evans, J. S., et al. (2015), Retrieval of CO₂ and N₂ in the Martian thermosphere using dayglow observations by IUVS on MAVEN, *Geophys. Res. Lett.*, 42, doi:10.1002/2015GL065489.

Received 21 JUL 2015

Accepted 1 OCT 2015

Retrieval of CO₂ and N₂ in the Martian thermosphere using dayglow observations by IUVS on MAVENJ. S. Evans¹, M. H. Stevens², J. D. Lumpe¹, N. M. Schneider³, A. I. F. Stewart³, J. Deighan³, S. K. Jain³, M. S. Chaffin³, M. Crismani³, A. Stiepen³, W. E. McClintock³, G. M. Holsclaw³, F. Lefèvre⁴, D. Y. Lo⁵, J. T. Clarke⁶, F. G. Eparvier³, E. M. B. Thiemann³, P. C. Chamberlin⁷, S. W. Bougher⁸, J. M. Bell⁹, and B. M. Jakosky³

¹Computational Physics, Inc., Springfield, Virginia, USA, ²Naval Research Laboratory, Washington, District of Columbia, USA, ³Laboratory for Atmospheric and Space Physics, University of Colorado Boulder, Boulder, Colorado, USA, ⁴LATMOS, CNRS, Paris, France, ⁵Lunar and Planetary Laboratory, University of Arizona, Tucson, Arizona, USA, ⁶Center for Space Physics, Boston University, Boston, Massachusetts, USA, ⁷NASA Goddard Space Flight Center, Greenbelt, Maryland, USA, ⁸Department of Atmospheric, Oceanic, and Space Sciences, University of Michigan, Ann Arbor, Michigan, USA, ⁹National Institute of Aerospace, Hampton, Virginia, USA

Abstract We present direct number density retrievals of carbon dioxide (CO₂) and molecular nitrogen (N₂) for the upper atmosphere of Mars using limb scan observations during October and November 2014 by the Imaging Ultraviolet Spectrograph on board NASA's Mars Atmosphere and Volatile Evolution (MAVEN) spacecraft. We use retrieved CO₂ densities to derive temperature variability between 170 and 220 km. Analysis of the data shows (1) low-mid latitude northern hemisphere CO₂ densities at 170 km vary by a factor of about 2.5, (2) on average, the N₂/CO₂ increases from 0.042 ± 0.017 at 130 km to 0.12 ± 0.06 at 200 km, and (3) the mean upper atmospheric temperature is 324 ± 22 K for local times near 14:00.

1. Introduction

Ultraviolet emissions from the Martian atmosphere provide an important means of inferring atmospheric composition [Meier, 1991; Paxton and Anderson, 1992]. The Martian UV airglow was first observed by the Mariner 6 and 7 missions in 1969 and subsequently by Mariner 9 in 1971–1972 [Barth et al., 1969, 1971; Stewart, 1972; Strickland et al., 1972; Stewart et al., 1972; Barth et al., 1972; Strickland et al., 1973]. From these early missions, excitation processes resulting in UV emissions were found to include photolysis, electron impact, dissociative recombination, and solar resonant fluorescent scattering [Barth et al., 1971, 1972; Fox and Dalgarno, 1979].

More recently, the Spectroscopy for the Investigation of the Characteristics of the Atmosphere of Mars spectrometer on board Mars Express has made important UV airglow observations. These include the discovery of emission due to solar energetic particles [Bertaux et al., 2005a; Leblanc et al., 2006a; Brain et al., 2006; Leblanc et al., 2008; Dubinin et al., 2009; Ip, 2012] and chemiluminescence [Bertaux et al., 2005b, 2005c; Cox et al., 2008]. More detailed analyses have obtained N₂ emissions [Leblanc et al., 2006b; Jain and Bhardwaj, 2011] and ozone global climatology [Perrier et al., 2006].

NASA's Mars Atmosphere and Volatile Evolution (MAVEN) spacecraft was launched on 18 November 2013 and arrived at Mars on 22 September 2014. The primary goal of the MAVEN mission is to quantify the diurnal, latitudinal, seasonal, and solar activity variations in the Martian atmosphere and to use that knowledge to determine the present and historical rates of escape of the Martian atmosphere [Jakosky et al., 2015]. To that end, we present a first attempt to directly retrieve CO₂ and N₂ densities in the Martian thermosphere from the mid-ultraviolet (MUV) dayglow. We use limb observations from 130 to 200 km tangent altitude by the Imaging Ultraviolet Spectrograph (IUVS) [McClintock et al., 2014] on board MAVEN. We compare our retrievals to results from the Mars-Global Ionosphere-Thermosphere Model (M-GITM) [Bougher et al., 2015], as well as in situ measurements by Vikings 1 and 2 [Nier and McElroy, 1977], and quantify the differences throughout the altitude region of interest.

We first discuss IUVS limb scan observations and the associated geographic and temporal coverage followed by a discussion of the forward model and optimal estimation techniques used herein. We then present the methodology used for direct retrievals of CO₂ and N₂ densities and deriving temperatures from CO₂ density profiles. We also explore the implications of forward model and calibration systematic uncertainties on density retrievals. In the final section, we summarize the most significant results of this study.

2. Observations

IUVS is designed to provide global 3-D maps of major molecules, atoms, and ions in the atmosphere [McClintock *et al.*, 2014; Jakosky *et al.*, 2015]. The instrument is a UV imaging spectrograph with a $10 \times 0.06^\circ$ slit and occultation apertures at each end. The MAVEN orbit is elliptical with apoapsis at ~ 6200 km and periapsis nominally at an altitude of ~ 175 km. Nadir viewing allows for disk maps near apoapsis, while limb viewing allows for scans near periapsis [Jain *et al.*, 2015]. IUVS measures the far ultraviolet (FUV) airglow on Mars between 110 and 190 nm at ~ 0.6 nm resolution and the MUV airglow between 180 and 340 nm at ~ 1.2 nm resolution. The vertical resolution is 5 km [McClintock *et al.*, 2014].

We use 82 dayglow limb scan observations constrained to solar zenith angles (SZAs) $< 60^\circ$ made by IUVS during MAVEN orbits 109–128 on 18–22 October 2014 and orbits 261–269 on 16–18 November 2014. These observations span northern hemisphere latitudes from -5° to 35° and all longitudes. Local times cluster near 14:00 and 11:00 for orbits 109–128 and 261–269, respectively; SZAs range from 30° to 60° . We use two types of MUV emission for our retrievals: the CO_2^+ Ultraviolet Doublet (UVD, 288–289 nm) produced primarily by photoionization and the N_2 Vegard-Kaplan bands (VK, 258 – 287 nm) produced exclusively by photoelectron excitation. Limb profiles of these blended emission features are extracted from calibrated data using multiple linear regression (MLR) techniques described by Stevens *et al.* [2015a].

3. Forward Model

The Atmospheric Ultraviolet Radiance Integrated Code (AURIC) software package was developed for upper atmospheric radiance modeling from the FUV to the near-infrared [Strickland *et al.*, 1999]. AURIC has been used to study the extreme ultraviolet (EUV) dayglow from the Earth [Bishop *et al.*, 2007], Titan [Strobel *et al.*, 1991, 1992; Stevens *et al.*, 2015b], Triton [Strobel *et al.*, 1991; Stevens, 2002], and Pluto [Schindhelm *et al.*, 2015].

The molecular states associated with the emissions of CO_2 and N_2 that are of interest here are produced by processes related to energetic solar irradiance: photoelectron excitation, photodissociative excitation and photodissociative ionization [Meier, 1991; Samson *et al.*, 1991; Bishop and Feldman, 2003]. The starting point for these processes is the unattenuated solar flux as a function of wavelength λ , $\pi F_o(\lambda_i)$, where λ_i refers to the i th solar irradiance wavelength in $\text{photons cm}^{-2} \text{s}^{-1} \text{nm}^{-1}$. The wavelength range of interest for nonresonant excitation is from ~ 100 nm down to 1 nm. Solar energy at shorter wavelengths is deposited below ~ 100 km and is insignificant except under extreme solar activity [Fox, 2004b].

The flux at altitude z and for $\mu_s = \cos(\text{SZA})$ is related to the unattenuated flux by

$$\pi F(\lambda_i, z, \mu_s) = \pi F_o(\lambda_i) \exp[-\tau(\lambda_i, z, \mu_s)]. \quad (1)$$

The optical depth, τ , is given by

$$\tau(\lambda_i, z, \mu_s) = \sum_l \tau_l(\lambda_i, z, \mu_s) = \sum_{lk} \sigma_{lk}^{\text{photo}}(\lambda_i) \int n_l(s) ds \quad (2)$$

where n_l is the density of the l th species and $\sigma_{lk}^{\text{photo}}(\lambda_i)$ is the wavelength-dependent photoabsorption cross section for channel k of species l . The integration in equation (2) is from the top of the atmosphere to altitude z along a slant path defined by μ_s . Although AURIC performs multistream photoelectron transport calculations, application of the model to limb scan retrievals is restricted to SZAs less than 60° , since anisotropy effects become increasingly important near the terminator. The photoabsorption cross sections (dissociation and ionization) in equation (2) come from the compilation of Conway [1988] for N_2 and molecular oxygen (O_2); from Bell and Stafford [1992] for atomic oxygen; and from Gronoff *et al.* [2012a] for CO_2 , carbon monoxide, argon, molecular hydrogen, helium, and atomic hydrogen.

The production of ionic or neutral states by absorption of photons from the solar flux $\pi F(\lambda_i, z, \mu_s)$ is given by

$$\delta p_{lki}(z, \mu_s) = n_l(z) \pi F(\lambda_i, z, \mu_s) \sigma_{lk}^{\text{photo}}(\lambda_i). \quad (3)$$

The accompanying expression for production of photoelectrons is

$$\delta p_{S_{lki}}(z, \mu_s, h\nu_i - I_{lk}) = n_l(z) \pi F(\lambda_i, z, \mu_s) \sigma_{lk}^{\text{photo}}(\lambda_i) \quad (4)$$

where $h\nu_i - I_{jk}$ is the energy of the photoelectron. Treatment of K-shell ionization and production of Auger electrons is explicitly included, as described by *Strickland et al.* [1999]. The total production rate summed over all solar lines capable of producing a specified state is

$$p_{jk}(z) = n_l(z) \sum_i \pi F(\lambda_i, z) \sigma_{jk}^{\text{photo}}(\lambda_i) \text{ cm}^{-3} \text{ s}^{-1}. \quad (5)$$

Production by electron impact is given by

$$p_{e,jk}(z) = n_l(z) \int_{W_{jk}}^{E_{\text{max}}} \sigma_{jk}(E) \phi(z, E) dE \text{ cm}^{-3} \text{ s}^{-1}, \quad (6)$$

where $\sigma_{jk}(E)$ is the electron impact cross section producing state k of species l by electrons at energy E , $\phi(z, E)$ is the spherically integrated photoelectron flux ($\text{cm}^{-2} \text{ s}^{-1} \text{ eV}^{-1}$), and W_{jk} is the threshold (eV).

We use a representative level 3 solar irradiance (energy flux of $1.9 \text{ ergs cm}^{-2} \text{ s}^{-1}$ over 1–45 nm) measured on 19 October 2014 by the Extreme UltraViolet Monitor (EUVM) on board MAVEN as reported by *Eparvier* [2015]. The level 3 product is a 1 nm modeled solar spectrum from 0.5–190.5 nm derived using three calibrated solar irradiance bands measured by EUVM. The solar irradiance is rebinned to a finer wavelength grid (equal apportionment of energy flux across subbins using 0.05 nm resolution from 1–10 nm and 0.1 nm from 10–105 nm) for use in our forward model calculations. Our analysis is not sensitive to the rebinning scheme as long as total energy flux within each EUVM bin is conserved in the rebinned spectrum. During the observations considered here, the Sun was moderately active producing one coronal mass ejection and multiple flares, including an X1.1 flare on 19 October 2014.

The CO_2^+ UVD ($\text{B } ^2\Pi_u^+ \rightarrow \text{X } ^2\Pi_g$) transition is allowed and the main sources are photoionization and electron impact ionization of CO_2 . Equation (5) is used to calculate the photoionization production rate, whereas equation (6) is used to calculate the electron impact ionization production rate. Photoionization of CO_2 is by far the dominant source of UVD at altitudes below $\sim 240 \text{ km}$ [*Fox and Dalgarno*, 1979; *Jain and Bhardwaj*, 2012]. We omit fluorescent scattering of sunlight by CO_2^+ , since it contributes less than 10% to the total UVD emission at altitudes below $\sim 200 \text{ km}$ [*Fox and Dalgarno*, 1979; *Fox*, 2004a, 2004b; *Jain and Bhardwaj*, 2012; *Stiepen et al.*, 2015]. Because UVD is emitted at 288–289 nm in a region of negligible pure absorption, accurate modeling of this transition is achievable to within the combined uncertainties of the relevant photoabsorption and photoionization cross sections and the assumed solar irradiance.

The volume production rate of the N_2 VK ($\text{A } ^3\Sigma_u^+ \rightarrow \text{X } ^3\Sigma_g^+$) transition, which derives exclusively from photoelectron impact excitation, is obtained from equation (6). However, the N_2 A state undergoes radiative cascade, intrasystem cascading, and electronic quenching [*Trajmar et al.*, 1983; *Morrill and Benesch*, 1996; *Jain and Bhardwaj*, 2011]. For modeling N_2 VK emission, we adopt the quenching parameters of *Gronoff et al.* [2012b]. Previous terrestrial work using AURIC showed that modeled N_2 VK emission is in good agreement with observations [*Strickland et al.*, 1999]. Analyses of Titan dayglow data using AURIC shows that observed N_2 VK emissions are in excellent agreement with model results in retrievals constrained only by photofragmented features [*Stevens et al.*, 2015b].

We use a spectral model of CO_2^+ UVD in AURIC to retrieve brightness profiles from IUVS observations [see *Stevens et al.*, 2015a]. In our model, we assume the $\text{B}(0,0,0)^2\Sigma_u^+ \rightarrow \text{X}(0,0,0)^2\Pi_g$ transition is the dominant contributor to the spectrum and that rovibrational effects due to perturbations by other vibronic states can be ignored. We use rotational term value parameters reported by *Farley and Cattolica* [1996] and Hönl-London factors from *Earls* [1935]. For modeling N_2 VK emission spectra, we use the band model described in *Stevens et al.* [2015a]. Vibrational populations of the N_2 ($\text{A } ^3\Sigma_u^+$) state for progressions $v' = 0\text{--}10$ are adopted from *Strickland et al.* [1999]. Relative populations are those reported by *Morrill and Benesch* [1996]. For the N_2 VK electron impact emission cross section, we use a sum of direct production cross sections of *Cartwright et al.* [1977] as discussed by *Daniell and Strickland* [1986].

4. Retrieval Algorithm

We infer atmospheric composition from IUVS measurements using the Generalized Retrieval and Analysis Tool. This tool merges AURIC with OPTimal estimation (hereafter OPT) retrieval algorithms [*Lumpe et al.*, 1997, 2002, 2007] and has already been applied to dayglow observations of Titan for the retrieval of N_2 and methane (CH_4) [*Stevens et al.*, 2015b]. We herein adapt the Titan algorithm to the Martian dayglow.

In the spectral dimension we convolve AURIC model spectra at 0.1 nm resolution for each tangent altitude with an IUVS point spread function as well as a slit function. We sum over all AURIC model spectral bins associated with chosen passbands for CO₂⁺ UVD and N₂ VK molecular band systems. For vertical smoothing we use a box car average, which yields an effective resolution of ~5 km and is consistent with the vertical resolution of the observations. Our forward model calculations assume that the atmosphere is spherically symmetric along the line of sight, which is a safe approximation at Mars for solar zenith angles below 60°.

The forward model problem is stated in general form as $y = F(x)$, where y represents the measurement vector of limb radiance profiles, x is the atmospheric state vector to be retrieved, and the full forward model F is defined by the combination of AURIC and an IUVS instrument model. This nonlinear equation is solved using the optimal estimation technique [Rodgers, 2000], with the solution vector \hat{x} obtained by iterating from the a priori vector x_a according to

$$\hat{x}_{n+1} = x_a + S_a K_n^T (K_n S_a K_n^T + S_y)^{-1} [y - y_n + K_n (\hat{x}_n - x_a)] \quad (7)$$

In equation (7) $y_n = F(x_n)$, S_y and S_a are the data and a priori covariance matrices, respectively, and the kernel matrix K_n is the derivative of the forward model with respect to the state parameters

$$K_n \equiv \left. \frac{\partial F}{\partial x} \right|_{x=x_n} \quad (8)$$

The covariance of the solution is a weighted sum of uncertainties from the a priori contribution and direct inversion of the data

$$\hat{S} = (S_a^{-1} + K^T S_y^{-1} K)^{-1} \quad (9)$$

The 1- σ retrieval uncertainties reported here are the diagonal elements of the retrieval covariance matrix: $\sigma_i \sim \sqrt{\hat{S}_{ii}}$. Since this approach is strictly formal uncertainty propagation, it may underestimate the true errors, which must be derived through a detailed uncertainty analysis using simulations to quantify individual uncertainty components.

5. Results

5.1. Density Profile Retrievals

The algorithms used in this analysis sequentially retrieve CO₂ and N₂ density profiles by fitting IUVS limb scan data. The density retrievals use a total of 20 (16) parameters for each CO₂⁺ UVD (N₂ VK) limb scan: constituent densities on a fixed altitude grid (19 grid points for CO₂ and 15 points for N₂) and a forward model brightness scale factor. The retrieval altitude grid uses equally spaced increments of 10 km from 80 to 150 km for CO₂ and 80 to 190 km for N₂ and an exponential grid up to 600 km. We find that the forward model is insensitive to variations in CO₂ and N₂ densities below the peak of volume production (nominally ~130 km for SZA < 60°) and above ~220 km.

As shown by Picone [2008], the influence of systematic biases on compositional retrievals from UV airglow is mitigated by scale factors. Forward model brightness scale factors are used to compensate for systematic biases between observed brightness profiles and values calculated by AURIC. These biases primarily arise from uncertainties in instrument calibration, cross sections used in AURIC, and solar XUV irradiance. IUVS MUV calibration uncertainties are estimated to be $\pm 30\%$, cross section uncertainties are reported to be $\pm 25\%$ [Avakyan et al., 1998; Majeed and Strickland, 1997], and EUVM level 3 daily irradiance uncertainties are $\pm 32\%$ [Eparvier, 2015]. We find that the retrieved CO₂⁺ UVD forward model scale factor has a mean value of 0.6 ± 0.1 , whereas the retrieved N₂ VK scale factor has a mean value of 1.02 ± 0.24 . These are both within the combined systematic uncertainties of the biases listed above (see section 5.3).

Retrieved forward model brightness profiles are calculated from CO₂ and N₂ densities obtained by modifying an a priori guess until a best fit solution is found. We use a priori values of 1.0 with a variance of 0.2 for the CO₂⁺ UVD and N₂ VK brightness scale factors. For observations with high signal-to-noise, scaling the variance up or down by a factor of 2 changes the retrieved CO₂ by at most a factor of 1.6 and N₂ by less than a factor of 1.4. A priori CO₂ and N₂ abundances for the density retrievals reported here are

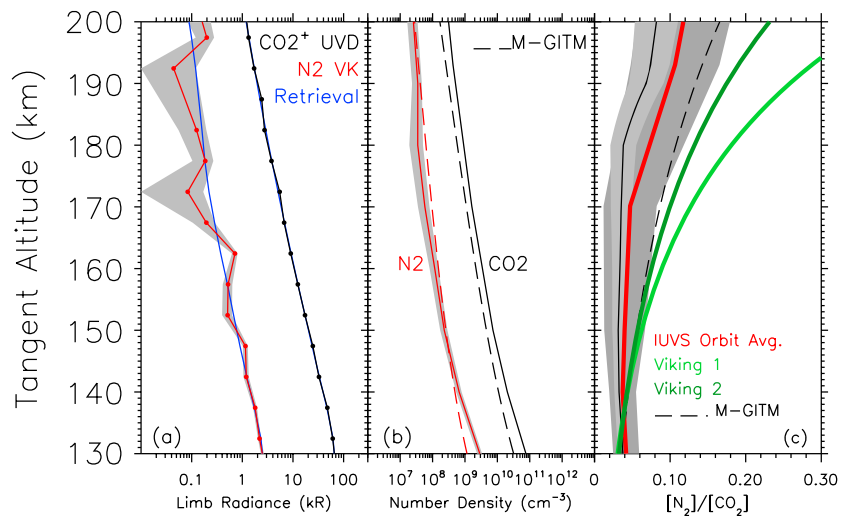


Figure 1. (a) CO_2^+ UVD (black) and the N_2 VK (red) brightness profiles observed by IUVS on 18 October 2014 at 16:44 UT during the tenth scan of MAVEN orbit 109 compared with retrieved forward model fits (blue). The mean satellite altitude for the scan was 319.4 km and the SZA was 42.5°. The shaded region designates a 1- σ standard deviation for the observation. (b) Retrieved CO_2 (black) and N_2 (red) density profiles compared to corresponding density profiles predicted by M-GITM for $L_s = 180$ (dashed). Random uncertainties for the retrieved densities are shown in the shaded region. (c) Retrieved N_2/CO_2 profile (solid black) compared with corresponding values predicted by M-GITM (dashed), Viking 1 (light green), Viking 2 (dark green), and the ensemble average of IUVS retrieved N_2/CO_2 for all scans considered herein (red). Shaded regions designate 1- σ standard deviations for single scan (light grey) and ensemble average (dark grey).

the mean of density profiles taken from the Mars Climate Database [Millour *et al.*, 2014] sampled over a full Martian year. Since CO_2 is the dominant source of photoelectrons in the Martian thermosphere, we perform CO_2 retrievals first and then use the retrieved density in the a priori atmosphere for N_2 retrievals (all other a priori species are unchanged). We find that scaling the a priori density up or down by a factor of 2 changes the retrieved CO_2 by a factor of 1.4 and N_2 by a factor of 1.2, where the retrievals are most sensitive to changes in density (130–220 km).

Figure 1a shows brightness profiles of CO_2^+ UVD and N_2 VK observed by IUVS on 18 October 2014 during the tenth scan of MAVEN orbit 109 (SZA = 44°; UT = 16:44; $F_{10.7} = 65$; latitude = 12°N; longitude = 131°E; s/c altitude = 320 km). The shaded region designates a 1- σ standard deviation for the observation. The MLR technique used to unblend and extract emission features from calibrated data is described in detail by Stevens *et al.* [2015a]. Comparisons of measured spectra with MLR retrieved composite synthetic spectra for the tenth scan of orbit 109 are illustrated in the supporting information in Figures S2 and S3. The overall agreement between retrieved forward model CO_2^+ UVD limb radiance profile and the data is better than 25% for tangent altitudes below 200 km. The ratio of forward model N_2 VK limb brightness to the observed brightness increases from a factor of 1.2 below 150 km to a factor of 2 at 200 km.

Figure 1b shows retrieved CO_2 and N_2 density profiles compared to corresponding density profiles predicted by M-GITM (dashed) [Bougher *et al.*, 2015] for L_s , $F_{10.7}$, latitude, and local solar time values of 180°, 130, 12.5°, and 14.2 h, respectively. The shaded region represents 1- σ retrieval uncertainties. CO_2 densities are in excess of model predictions by factors of 2 to 3 between 200 and 130 km, whereas a direct comparison of N_2 densities shows an overestimation by the model at and above 150 km and an underestimation below.

The quantity N_2/CO_2 can be used to assess the strength of vertical mixing in the Martian upper atmosphere, and the comparison of N_2/CO_2 with M-GITM-predicted values in Figure 1c contrasts with the separate comparison of N_2 and CO_2 densities in Figure 1b. The comparison of retrieved N_2/CO_2 with M-GITM results in Figure 1c clarifies the differences, indicating good agreement at 130 km, but an overestimation from the model by a factor of ~2 at 200 km. The increase in mean N_2/CO_2 with altitude reflects the fact that N_2 is in the diffusively separated region of the Martian atmosphere.

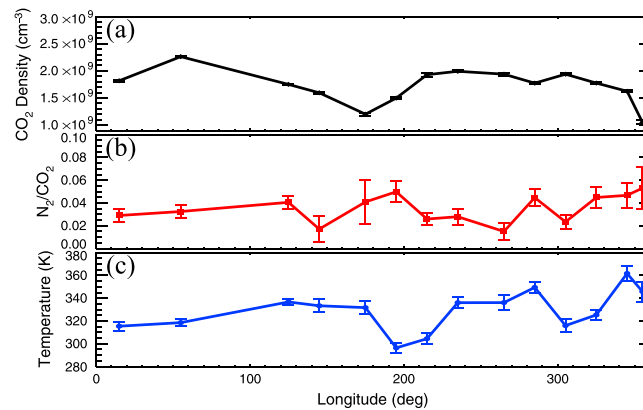


Figure 2. (a) Retrieved CO_2 density at an altitude of 170 km for 23 (out of 82) limb scans from orbit 109 on 18 October 2014 to orbit 269 on 18 November 2014 binned by latitude from -5° to 10° and by longitude every 10° . All points falling within each bin are averaged together with uncertainties rigorously propagated to derive the error bars shown in the figure. (b) Retrieved N_2/CO_2 binned by latitude and longitude. (c) Upper atmospheric temperature derived from fits to retrieved CO_2 density profiles over altitudes from 170 to 220 km binned by latitude and longitude (see text).

To determine if the single scan considered here is representative of overall behavior, we include in Figure 1c the ensemble average of N_2/CO_2 from 82 limb scans. Figure 1c shows that our sample N_2/CO_2 profile from orbit 109 is lower than the ensemble average, but nearly within the $1\text{-}\sigma$ standard deviation of the geophysical variability. We find good agreement between the ensemble average and M-GITM predictions at 130 and 200 km, but an overall difference in the shape of the profiles, with a maximum difference of a factor of ~ 1.8 near 170 km.

Given the current state of analyses and data product generation, it is beyond the scope of this paper to conduct a detailed comparison of IUVS results with (nearly) coincident in situ data from the Neutral

Gas Ionizing Mass Spectrometer (NGIMS) [Mahaffy *et al.*, 2014] on board MAVEN. However, we can make qualitative comparisons of our results with previous in situ composition measurements by the Vikings 1 and 2 entry probes in 1976 [Nier and McElroy, 1977], which extended from ~ 200 km down to ~ 120 km. These data are included in Figure 1c as least squares fits to N_2/CO_2 (assuming the ratio varies exponentially with altitude). The Viking data suggest that the homopause should be located between 120 and 130 km. However, the data also suggest that the atmosphere sampled by Viking 1 was statically more stable than that sampled by Viking 2; thus, the homopause sampled by Viking 2 was higher than that seen by Viking 1. The ensemble data presented here indicate that the mean atmosphere sampled by IUVS is well mixed to slightly higher levels than predicted by M-GITM, but consistent with the differences observed by Vikings 1 and 2, although this result should be examined with a larger MAVEN data set.

The recently revised N_2 mixing ratio at the Martian surface as measured by the Sample Analysis at Mars (SAM) experiment on the Curiosity rover of the Mars Science Laboratory mission is 0.0203 ± 0.0003 [Franz *et al.*, 2015]. Mahaffy *et al.* [2015] report that at altitudes near ~ 125 km N_2/CO_2 measured by NGIMS approaches the bulk atmospheric mixing ratio established by the SAM experiment. In contrast, both the IUVS and M-GITM N_2/CO_2 values near that altitude are about a factor of 2 higher than the surface value. More specifically, we find that the mean N_2/CO_2 increases from 0.042 ± 0.017 at 130 km to 0.12 ± 0.06 at 200 km. NGIMS values near the same altitudes are approximately 0.02 and 0.12, respectively [Mahaffy *et al.*, Figure 6]. It should be mentioned that the M-GITM results used here reflect assumed boundary conditions in the lower atmosphere. Thus, differences in M-GITM predictions with other measurements (Viking, NGIMS, or IUVS) require further study with a larger MAVEN data set.

Using an ensemble of retrievals for 23 (out of 82) limb scans, we can investigate the spatial variability of densities in the equatorial region covered by the available observations. In Figure 2a we show retrieved CO_2 densities corresponding to an altitude of 170 km as a function of longitude. The retrievals have been averaged over northern hemisphere latitudes from -5° to 35° and in 10° longitude bins. The CO_2 densities vary by over a factor of 2 ranging from 1×10^9 to $2.3 \times 10^9 \text{ cm}^{-3}$. Longitudinal structure in the densities is evident with maxima centered near 50° and 280° . If the dayglow at Mars has small temporal variations over the month of observations shown in Figure 2, this longitudinal structure may be a signature of tides in the Martian thermosphere [Lo *et al.*, 2015]. A similar degree of variability is evident in the ratio of retrieved N_2 and CO_2 shown in Figure 2b.

5.2. Temperature Retrievals

Following the approach of *Westlake et al.* [2011], we retrieve upper atmospheric temperatures at Mars by inferring scale heights from retrieved CO₂ density profiles between 170 and 220 km. We use a geopotential altitude to account for changes in gravitational acceleration with altitude. Considering all scans, we find a mean Martian temperature (reference altitude of 170 km) of 324 K with a 1- σ standard deviation of 22 K. Figure 2c shows spatially binned upper atmospheric temperatures as a function of longitude. The observed variation of ~ 60 K in temperature is considerable but consistent with values derived from previous observations [*Stewart, 1972; Stewart et al., 1972; Leblanc et al., 2006b; Stiepen et al., 2015*] and climate model predictions [*Bougher et al., 2009, 2015*]. We note that the mean temperature from our analysis agrees within the respective uncertainties with a temperature of 285.1 ± 21.7 K determined from changes in the density scale height of Argon (Ar) measured by NGIMS over the same time frame (see Figure S1 in the supporting information).

5.3. Systematic Uncertainty Analysis

It is evident from equations (5) and (6) that the main sources of forward model uncertainty are solar irradiance (energy input), total photoabsorption cross sections (attenuation), photoionization cross sections (ion and photoelectron production), and finally elastic and inelastic electron impact cross sections (ion production and energy loss). Additional uncertainties unrelated to the forward model include instrument pointing and calibration.

Through simulated retrievals we determined that the sensitivity of CO₂ densities to nonflare solar variability is negligible at and above the CO₂⁺ UVD emission peak, whereas the impact on N₂ retrievals is at most $\sim 25\%$. To quantify the sensitivity of density retrievals to more active solar conditions, we repeated the retrievals shown in Figure 1 with an alternative solar irradiance spectrum measured by EUVM 45 min after the X1.1 flare occurring on 19 October 2014 [*Thiemann et al., 2015*], with an energy flux 1.6 times the value from the representative solar irradiance used in this study that was measured by EUVM on 18 October 2014. We find that retrieved densities based on the postflare solar spectrum are reduced relative to preflare densities by at most a factor of 1.4 at altitudes above 140 km, with an increased effect at lower altitudes. The overall reduction in retrieved densities using the postflare solar spectrum compensates for the increased energy in the solar spectrum. The increased effect at lower altitudes is due to soft X-ray solar photons penetrating deeper in the atmosphere, thereby changing the shape of forward model emission profiles near and below the emission peak. While not critical, it is best to use a solar irradiance that is appropriate for the solar activity during which dayglow observations are made.

IUVS was calibrated against UV-bright stars and scaled by instrument geometric factors appropriate for extended source observations. The MUV systematic uncertainty estimated from these stellar calibrations is $\pm 30\%$. We find that a 30% reduction in the absolute calibration has a negligible impact on the retrieval of CO₂ densities but leads to a 30% reduction in retrieved N₂ densities. In the former case, it is the altitude distribution of the observed CO₂⁺ UVD limb brightness profile, rather than the magnitude, that is directly diagnostic of the CO₂ density profile. Specifically, the height of the peak of emission corresponds to an absolute CO₂ density, and the relative shape of the CO₂⁺ UVD limb profile above the peak describes the CO₂ scale height. This behavior is expected when considering the expression for volume production of CO₂⁺ UVD given by equation (5). The estimated pointing accuracy of MAVEN is 5 km on the limb [*McClintock et al., 2014*]. This corresponds to a factor of 2 uncertainty in retrieved CO₂ densities due to the direct relationship between CO₂⁺ UVD emission peak altitude and absolute density at the emission peak. We therefore conclude that the dominant uncertainty in retrieved CO₂ densities is pointing accuracy.

In contrast, equation (6) suggests that the 30% instrument calibration uncertainty propagates directly to N₂ retrievals since there is a linear relationship between the N₂ density and the N₂ VK brightness. This is because VK is produced exclusively by photoelectrons exciting N₂ that result predominately from photoionization of CO₂. The total systematic uncertainty in the retrieved N₂ densities is a combination of instrument calibration, solar irradiance, and cross sections, although the total N₂ uncertainty is mitigated by a scale factor used in the retrieval [*Stevens et al., 2015b*]. A complete uncertainty analysis of the IUVS limb scan retrieval data products will be presented in a forthcoming algorithm paper.

6. Conclusions

We have presented the first direct retrievals of CO₂ and N₂ number densities in Mars' upper atmosphere using MUV dayglow observations from 130 to 200 km. We use two MUV emission features observed by IUVS on MAVEN for our retrievals: CO₂⁺ UVD and N₂ VK. The dominant source of UVD is photoionization of CO₂, and so the emission is directly diagnostic of CO₂ density variations. Similarly, N₂ VK emission is produced exclusively by photoelectron impact and is diagnostic of N₂ density variations. It is worth noting that neither of the selected emission features is affected by pure absorption over the range of tangent altitudes reported here.

Key findings in this study are

1. CO₂ densities at 170 km vary by a factor of about 2.5 over a month of observations in October and November 2014.
2. The N₂/CO₂ indicates that N₂ is in the diffusively separated region of the Martian atmosphere with a mean ratio that increases from 0.042 ± 0.017 at 130 km to 0.12 ± 0.06 at 200 km.
3. The mean Martian upper atmospheric temperature over the sampled time frame is 324 ± 22 K.

We also find that CO₂ and N₂ density retrievals from MUV limb scan observations at Mars are insensitive to quiet time variability in solar irradiance, but care must be taken to use appropriate flare spectra during active times. Finally, CO₂ density retrievals from MUV limb scan observations at Mars are insensitive to instrument calibration and instead are primarily sensitive to the accuracy of the pointing, while instrument calibration errors propagate directly to errors in N₂ retrievals. Observed densities that are a factor of 3 less than predictions as suggested by some previous studies [e.g., *Leblanc et al.*, 2007; *Simon et al.*, 2009; *Jain and Bhardwaj*, 2011] are not supported by the comparisons presented herein [see also *Stevens et al.*, 2015a].

IUVS observations over additional months will provide valuable insight to seasonal variations of CO₂ and N₂ in the Martian upper atmosphere. In addition, a variety of other emissions [*Jain et al.*, 2015] will be used to quantify spatial and temporal variations of composition in the Martian upper atmosphere.

Acknowledgments

The MAVEN project is supported by NASA through the Mars Exploration Program. J.S.E. acknowledges support from the University of Colorado Laboratory for Atmospheric and Space Physics and thanks John Correia for his assistance in generating figures for this paper. M.H.S. was supported by the NASA MAVEN Participating Scientist program. A. Stiepen is supported by the Belgian American Educational Foundation and the Rotary District 1630. The IUVS processing pipeline automatically generates level 2 retrieval data products, which are stored at the Planetary Atmospheres Node of the Planetary Data System (http://atmos.nmsu.edu/data_and_services/atmospheres_data/MAVEN/maven_iuvs.html). Data files can be identified by file names with the orbit numbers given, the word "periapse," and the identifier v03_r01. Data release v03_r01 includes CO₂ and N₂ density profiles and upper atmosphere temperatures. Later releases will include additional species and derived quantities.

References

- Avakyan, S. V., R. N. Il'in, V. M. Lavrov, and G. N. Ogurtsov (Eds) (1998), *Collision Processes and Excitation of UV Emission From Planetary Atmospheric Gases: A Handbook of Cross Sections*, Gordon and Breach, Amsterdam.
- Barth, C. A., W. G. Fastie, C. W. Hord, J. B. Pearce, K. K. Kelly, A. I. Stewart, G. E. Thomas, G. P. Anderson, and O. F. Raper (1969), Mariner 6: ultraviolet spectrum of Mars upper atmosphere, *Science*, *165*, 1004–1005.
- Barth, C. A., C. W. Hord, J. B. Pearce, K. K. Kelly, G. P. Anderson, and A. I. Stewart (1971), Mariner 6 and 7 ultraviolet spectrometer experiment: Upper atmosphere data, *J. Geophys. Res.*, *76*, 2213–2227, doi:10.1029/JA076i010p02213.
- Barth, C. A., A. I. Stewart, and C. W. Hord (1972), Mars airglow spectroscopy and variations in Lyman alpha, *Icarus*, *17*, 457–468.
- Bell, K. L., and R. P. Stafford (1992), Photoionization cross-sections for atomic oxygen, *Planet. Space Sci.*, *40*, 1419.
- Bertaux, J.-L., F. Leblanc, O. Witasse, E. Quemerais, J. Liliensten, S. A. Stern, B. Sandel, and O. Korabev (2005a), Discovery of an aurora on Mars, *Nature*, *435*, 790–794.
- Bertaux, J.-L., F. Leblanc, S. Perrier, E. Quemerais, O. Korabev, F. Forget, D. Fonteyn, S. A. Stern, and B. Sandel (2005b), Detection of Martian nightglow: NO recombination bands and aurora over crustal magnetic anomalies, *AGU Fall Meeting Abstracts*, p. A7.
- Bertaux, J.-L., et al. (2005c), Nightglow in the upper atmosphere of Mars and implications for atmospheric transport, *Science*, *307*, 566–569.
- Bishop, J., and P. D. Feldman (2003), Analysis of the Astro-1/Hopkins Ultraviolet Telescope EUV/FUV dayside nadir spectral radiance measurements, *J. Geophys. Res.*, *108*(A6), 1243, doi:10.1029/2001JA000330.
- Bishop, J., M. H. Stevens, and P. D. Feldman (2007), Molecular nitrogen Carroll-Yoshino $v' = 0$ emission in the thermospheric dayglow as seen by the Far Ultraviolet Spectroscopic Explorer, *J. Geophys. Res.*, *112*, A10312, doi:10.1029/2007JA012389.
- Bougher, S. W., T. M. McDunn, K. A. Zoldak, and J. M. Forbes (2009), Solar cycle variability of Mars dayside exospheric temperatures: Model evaluation of underlying thermal balances, *Geophys. Res. Lett.*, *36*, L05201, doi:10.1029/2008GL036376.
- Bougher, S. W., D. Pawlowski, J. M. Bell, S. Nelli, T. McDunn, J. R. Murphy, M. Chizek, and A. Ridley (2015), Mars Global Ionosphere-Thermosphere Model: Solar cycle, seasonal, and diurnal variations of the Mars upper atmosphere, *J. Geophys. Res. Planets*, *120*, 311–342, doi:10.1002/2014JE004715.
- Brain, D. A., J. S. Halekas, L. M. Peticolas, R. P. Lin, J. G. Luhmann, D. L. Mitchell, G. T. Delory, S. W. Bougher, M. H. Acuña, and H. Rème (2006), On the origin of aurorae on Mars, *Geophys. Res. Lett.*, *33*, L01201, doi:10.1029/2005GL024782.
- Cartwright, D. C., S. Trajmar, A. Chutjian, and W. Williams (1977), Electron impact excitation of the electronic states of N₂, II, Integral cross sections at incident energies from 10 to 50 eV, *Phys. Rev. A*, *16*, 1041–1051.
- Conway, R. R. (1988), NRL Memorandum Report 6155 Naval Research Laboratory, Washington, D. C.
- Cox, C., A. Saglam, J.-C. Gérard, J.-L. Bertaux, F. González-Galindo, F. Leblanc, and A. Reberac (2008), Distribution of the ultraviolet nitric oxide Martian night airglow: Observations from Mars Express and comparisons with a one-dimensional model, *J. Geophys. Res.*, *113*, E08012, doi:10.1029/2007JE003037.
- Daniell, R. E., and D. J. Strickland (1986), Dependence of auroral middle UV emissions on the incident electron spectrum and neutral atmosphere, *J. Geophys. Res.*, *91*, 321–327, doi:10.1029/JA091iA01p00321.

- Dubinin, E., M. Fraenz, J. Woch, S. Barabash, and R. Lundin (2009), Long-lived auroral structures and atmospheric losses through auroral flux tubes on Mars, *Geophys. Res. Lett.*, *36*, L08108, doi:10.1029/2009GL038209.
- Earls, L. T. (1935), Intensities in ${}^2\Pi \rightarrow {}^2\Sigma$ transitions in diatomic molecules, *Phys. Rev.*, *48*, 423–424.
- Eparvier, F. G. (2015), The solar extreme ultraviolet monitor for MAVEN, *Space Sci. Rev.*, doi:10.1007/s11214-015-0195-2.
- Farley, D. R., and R. J. Cattolica (1996), Electron-beam fluorescence from the $A^2\Pi_u \rightarrow X^2\Pi_g$ and $B^2\Sigma_u^+ \rightarrow X^2\Pi_g$ transitions of CO_2^+ , *J. Quant. Spectrosc. Radiat. Transfer*, *56*, 83–96.
- Fox, J. L. (2004a), CO_2^+ dissociative recombination: A source of thermal and nonthermal C on Mars, *J. Geophys. Res.*, *109*, A08306, doi:10.1029/2004JA010514.
- Fox, J. L. (2004b), Response of the Martian thermosphere/ionosphere to enhanced fluxes of solar soft X-rays, *J. Geophys. Res.*, *109*, A11310, doi:10.1029/2004JA010380.
- Fox, J. L., and A. Dalgarno (1979), Ionization, luminosity, and heating of the upper atmosphere of Mars, *J. Geophys. Res.*, *84*, 7315–7333, doi:10.1029/JA084iA12p07315.
- Franz, H., M. Trainer, M. Wong, P. Mahaffy, S. Atreya, H. Manning, and J. Stern (2015), Reevaluated Martian atmospheric mixing ratios from the mass spectrometer on the Curiosity rover, *Planet. Space Sci.*, *109–110*, 154–158.
- Gronoff, G., C. S. Wedlund, C. J. Mertens, M. Barthélemy, R. J. Lillis, and O. Witasse (2012a), Computing uncertainties in ionosphere-airglow models: I. Electron flux and species production uncertainties for Mars, *J. Geophys. Res.*, *117*, A04306, doi:10.1029/2011JA016930.
- Gronoff, G., C. S. Wedlund, C. J. Mertens, M. Barthélemy, R. J. Lillis, and O. Witasse (2012b), Computing uncertainties in ionosphere-airglow models: II. The Martian airglow, *J. Geophys. Res.*, *117*, A05309, doi:10.1029/2011JA017308.
- Ip, W. H. (2012), ENA diagnostics of auroral activity at Mars, *Planet. Space Sci.*, *63*, 83–86.
- Jain, S. K., and A. Bhardwaj (2011), Model calculation of N_2 Vegard-Kaplan band emissions in Martian dayglow, *J. Geophys. Res.*, *116*, E07005, doi:10.1029/2010JE003778.
- Jain, S. K., and A. Bhardwaj (2012), Impact of solar EUV flux on CO Cameron band and CO_2^+ UV doublet emissions in the dayglow of Mars, *Planet. Space Sci.*, *63–64*, 110–122.
- Jain, S. K., et al. (2015), The structure and variability of Mars upper atmosphere as seen in MAVEN/IUVS dayglow observations, *Geophys. Res. Lett.*, *42*, doi:10.1002/2015GL065419.
- Jakosky, B. M., et al. (2015), The Mars Atmosphere and Volatile Evolution (MAVEN) Mission, *Space Sci. Rev.*, doi:10.1007/s11214-015-0139-x.
- Leblanc, F., O. Witasse, J. Winningham, D. Brain, J. Liliensten, P.-L. Blelly, R. A. Frahm, J. S. Halekas, and J. L. Bertaux (2006a), Origins of the Martian aurora observed by Spectroscopy for Investigation of Characteristics of the Atmosphere of Mars (SPICAM) on board Mars Express, *J. Geophys. Res.*, *111*, A09313, doi:10.1029/2006JA011763.
- Leblanc, F., J. Y. Chaufray, J. Liliensten, O. Witasse, and J.-L. Bertaux (2006b), Martian dayglow as seen by the SPICAM UV spectrograph on Mars Express, *J. Geophys. Res.*, *111*, E09511, doi:10.1029/2005JE002664.
- Leblanc, F., J. Y. Chaufray, and J. L. Bertaux (2007), On Martian nitrogen dayglow emission observed by SPICAM UV spectrograph/Mars Express, *Geophys. Res. Lett.*, *34*, L02206, doi:10.1029/2006GL028437.
- Leblanc, F., et al. (2008), Observations of aurorae by SPICAM ultraviolet spectrograph on board Mars Express: Simultaneous ASPERA-3 and MARSIS measurements, *J. Geophys. Res.*, *113*, A08311, doi:10.1029/2008JA013033.
- Lo, D. Y., et al. (2015), Non-migrating tides in the Martian atmosphere as observed by MAVEN IUVS, *Geophys. Res. Lett.*, *42*, doi:10.1002/2015GL066268.
- Lumpe, J. D., et al. (1997), POAM II retrieval algorithm and error analysis, *J. Geophys. Res.*, *102*, 23,593–23,614, doi:10.1029/97JD00906.
- Lumpe, J. D., R. M. Bevilacqua, K. W. Hoppel, and C. E. Randall (2002), POAM III retrieval algorithm and error analysis, *J. Geophys. Res.*, *107*(D21), 4575, doi:10.1029/2002JD002137.
- Lumpe, J. D., L. E. Floyd, L. C. Herring, S. T. Gibson, and B. R. Lewis (2007), Measurements of thermospheric molecular oxygen from the Solar Ultraviolet Spectral Irradiance Monitor, *J. Geophys. Res.*, *112*, D16308, doi:10.1029/2006JD008076.
- Mahaffy, P. R., et al. (2014), The neutral gas and ion mass spectrometer on the Mars atmosphere and volatile evolution mission, *Space Sci. Rev.*, doi:10.1007/s11214-014-0091-1.
- Mahaffy, P. R., M. Benna, M. Elrod, R. V. Yelle, S. W. Bougher, S. W. Stone, and B. M. Jakosky (2015), Structure and composition of the neutral upper atmosphere of Mars from the MAVEN NGIMS investigation, *Geophys. Res. Lett.*, *42*, doi:10.1002/2015GL065329.
- Majeed, T., and D. J. Strickland (1997), New survey of electron impact cross sections for photoelectron and auroral electron energy loss calculations, *J. Phys. Chem. Ref. Data*, *26*, 335–349.
- McClintock, W. E., N. M. Schneider, G. M. Holsclaw, J. T. Clarke, A. C. Hoskins, I. Stewart, F. Montmessin, R. V. Yelle, and J. Deighan (2014), The Imaging Ultraviolet Spectrograph (IUVS) for the MAVEN Mission, *Space Sci. Rev.*, doi:10.1007/s11214-014-0098-7.
- Meier, R. R. (1991), Ultraviolet spectroscopy and remote sensing of the upper atmosphere, *Space Sci. Rev.*, *58*, 1–185, doi:10.1007/BF01206000.
- Millour, E., et al. (2014), The Mars Climate Database (MCD version 5.1), LPI Contrib. 1791, 1184.
- Morrill, J. S., and W. M. Benesch (1996), Auroral N_2 emissions and the effect of collisional processes on N_2 triplet state vibrational populations, *J. Geophys. Res.*, *101*, 261–274, doi:10.1029/95JA02835.
- Nier, A. O., and M. B. McElroy (1977), Composition and structure of Mars' upper atmosphere: Results from the neutral mass spectrometers on Viking 1 and 2, *J. Geophys. Res.*, *82*(28), 4341–4349, doi:10.1029/J082i028p04341.
- Paxton, L. J., and D. E. Anderson (1992), Far ultraviolet remote sensing of Venus and Mars, in *Venus and Mars: Atmospheres, Ionospheres, and Solar Wind Interactions*, *Geophys. Monogr. Ser.*, vol. 66, edited by J. G. Luhmann, M. Tatralay, and R. O. Pepin, pp. 113–189, AGU, Washington D. C.
- Perrier, S., J. L. Bertaux, F. Lefevre, S. Lebonnois, O. Koroblev, A. Fedorova, and F. Montmessin (2006), Global distribution of total ozone on Mars from SPICAM/MEX UV measurements, *J. Geophys. Res.*, *111*, E09506, doi:10.1029/2006JE002681.
- Picone, J. M. (2008), Influence of systematic error on least squares retrieval of upper atmospheric parameters from the ultraviolet airglow, *J. Geophys. Res.*, *113*, A09306, doi:10.1029/2007JA012831.
- Rodgers, C. D. (2000), *Series on Atmospheric Oceanic and Planetary Physics*, World Sci., Singapore.
- Samson, J. A. R., Y. Chung, and E. M. Lee (1991), Excited ionic and neutral fragments produced by dissociation of the $\text{N}_2^+ \text{H}$ band, *J. Chem. Phys.*, *95*, 717–719.
- Schindhelm, E., S. A. Stern, R. Gladstone, and A. Zangari (2015), Pluto and Charon's UV spectra from IUE to New Horizons, *Icarus*, *246*, 206–212.
- Simon, C., O. Witasse, F. Leblanc, G. Gronoff, and J. L. Bertaux (2009), Dayglow on Mars: Kinetic modeling with SPICAM UV limb data, *Planet. Space Sci.*, *57*, 1008–1021.
- Stevens, M. H. (2002), The EUV Airglow of N_2 atmospheres, in *Atmospheres in the Solar System: Comparative Aeronomy*, *Geophys. Monogr.*, vol. 130, pp. 319–328, AGU, Washington, D. C.
- Stevens, M. H., et al. (2015a), New observations of molecular nitrogen in the Martian upper atmosphere by IUVS on MAVEN, *Geophys. Res. Lett.*, *42*, doi:10.1002/2015GL065319.

- Stevens, M. H., J. S. Evans, J. Lumpe, J. H. Westlake, J. M. Ajello, E. T. Bradley, and L. W. Esposito (2015b), Molecular nitrogen and methane density retrievals from Cassini UVIS dayglow observations of Titan's upper atmosphere, *Icarus*, *247*, 301–312.
- Stewart, A. I. (1972), Mariner 6 and 7 ultraviolet spectrometer experiment: Implications of CO_2^+ , CO and O airglow, *J. Geophys. Res.*, *77*, 54–68, doi:10.1029/JA077i001p00054.
- Stewart, A. I., C. Barth, and C. W. Hord (1972), Mariner 9 ultraviolet spectrometer experiment: Structure of Mars' upper atmosphere, *Icarus*, *17*, 469–474.
- Stiepen, A., J.-C. Gérard, S. Bougher, F. Montmessin, B. Hubert, and J. L. Bertaux (2015), Mars thermospheric scale height: CO Cameron and CO_2^+ dayglow observations from Mars Express, *Icarus*, *245*, 295–305, doi:10.1016/j.icarus.2014.09.051.
- Strickland, D. J., G. E. Thomas, and P. R. Sparks (1972), Mariner 6 and 7 ultraviolet spectrometer experiment: Analysis of the O I 1304 Å and 1356 Å emissions, *J. Geophys. Res.*, *77*, 4052–4068, doi:10.1029/JA077i022p04052.
- Strickland, D. J., A. I. Stewart, C. A. Barth, C. W. Hord, and A. L. Lane (1973), Mariner 9 ultraviolet spectrometer experiment: Mars atomic oxygen 1304-Å emission, *J. Geophys. Res.*, *78*, 4547–4559, doi:10.1029/JA078i022p04547.
- Strickland, D. J., J. Bishop, J. S. Evans, T. MAjeed, P. M. Shen, R. J. Cox, R. Link, and R. E. Huffman (1999), Atmospheric ultraviolet radiance integrated code (AURIC): Theory, software architecture, inputs, and selected results, *J. Quant. Spectrosc. Radiat. Transfer*, *62*, 689–742, doi:10.1016/S0022-4073(98)00098-3.
- Strobel, D. F., R. R. Meier, M. E. Summers, and D. J. Strickland (1991), Nitrogen airglow sources: Comparison of Triton, Titan, and Earth, *Geophys. Res. Lett.*, *18*, 689–692, doi:10.1029/91GL00133.
- Strobel, D. F., M. E. Summers, and X. Zhu (1992), Titan's upper atmosphere: Structure and ultraviolet emissions, *Icarus*, *100*, 512–526.
- Thiemann, E. M. B., et al. (2015), Neutral density response to solar flares at Mars, *Geophys. Res. Lett.*, *42*, doi:10.1002/2015GL066334.
- Trajmar, S., D. F. Register, and A. Chutjian (1983), Electron scattering by molecules II. Experimental methods and data, *Phys. Rep.*, *97*, 220–356.
- Westlake, J. H., J. M. Bell, J. H. Waite Jr., R. E. Johnson, J. G. Luhmann, K. E. Mandt, B. A. Magee, and A. M. Rymer (2011), Titan's thermospheric response to various plasma environments, *J. Geophys. Res.*, *116*, A03318, doi:10.1029/2010JA016251.